



# 13<sup>TH</sup> IEEE CEFC 2008

Athens, 11-15 May 2008

[Booklet](#)

[Program](#)

[Digests](#)

[Authors' Index  
by Page](#)

[Authors' Index  
by Session](#)

[Search](#)

MAIN

	<b>nerator for Wave Power Generation</b>	
	<i>Su-Kwon Jeong, Ki-Bong Jang, Gyu-Tak Kim</i> CHANGWON NATIONAL UNIVERSITY, KOREA	
PF1-4	<b>A Design for Improving Efficiency through Analyzing Characteristics of Single Phase Line-start Permanent Magnet Motor for Household Appliance</b>	492
	<i>Byeong-Hwa Lee<sup>1</sup>, Fan Glang<sup>1</sup>, Jung-Pyo Hong<sup>1</sup>, Hyuk Nam<sup>1</sup>, Seung-Hyung Ha<sup>2</sup></i> <sup>1</sup> HANYANG UNIVERSITY, KOREA, <sup>2</sup> LG ELECTRONICS INC., KOREA	
PF1-5	<b>Improved Physics-Based Permanent Magnet Synchronous Machine Model Obtained From Field Computation</b>	493
	<i>S. Liu, O. A. Mohammed, Z. Liu</i> FLORIDA INTERNATIONAL UNIVERSITY, USA	
PF1-6	<b>Modeling of Magnetoelastic and Piezoelectric Coupling: Application to SRM Noise Damping</b>	494
	<i>X. Mininger, N. Galopin, X. Ojeda, F. Bouillault, M. Gabsi</i> LABORATOIRE DE GENIE ELECTRIQUE DE PARIS-CNRG, FRANCE	
PF1-7	<b>Extraction of Effective Permittivity and Permeability of Metallic Powders in the Microwave Range</b>	495
	<i>Tomasz Galek, Ursula van Rienen</i> ROSTOCK UNIVERSITY, GERMANY	
PF1-8	<b>On the Design Optimization of Multilayer Microwave Absorbers</b>	496
	<i>Charalambos A. Stergiou<sup>1</sup>, Athanasios Oikonomou<sup>1</sup>, Tania Giannakopoulou<sup>2</sup>, George Litsardakis<sup>1</sup></i> <sup>1</sup> ARISTOTLE UNIVERSITY OF THESSALONIKI, GREECE, <sup>2</sup> NCSR "DEMOCRITOS", GREECE	
PF1-9	<b>Analysis and Measurements of Iron Loss and Interlinkage Flux inside Silicon Steel Lamination</b>	497
	<i>Z. Cheng<sup>1</sup>, N. Takahashi<sup>2</sup>, B. Forghani<sup>3</sup>, G. Gilbert<sup>3</sup>, J. Zhang<sup>1</sup>, L. Liu<sup>1</sup>, Y. Fan<sup>1</sup>, X. Zhang<sup>1</sup>, G. Han<sup>1</sup>, J. Wang<sup>1</sup>, C. Jiao<sup>1</sup></i> <sup>1</sup> BACDING TIANWEI GROUP CO., P.R. CHINA, <sup>2</sup> OKAYAMA UNIVERSITY, JAPAN, <sup>3</sup> INFOLYTICA CORP., CANADA	
PF1-10	<b>Finite Element Assisted Method of Estimating Equivalent Circuit Parameters for a Superconducting Synchronous Generator with a Coreless Rotor</b>	498
	<i>Bartosz Lukaszik, Kevin F. Goddard, Jan K. Sykulski</i> UNIVERSITY OF SOUTHAMPTON, UK	
PF1-11	<b>Numerical Investigations on Inductive Method for Film/Bulk Superconductors</b>	499
	<i>Atsushi Kamitani, Terou Takayama, Soichiro Ikuno</i> YAMAGATA UNIVERSITY, JAPAN	
PF1-12	<b>Transient Simulation and Analysis for Three-Phase Saturated Core High Temperature Superconducting Fault Current Limiter</b>	500
	<i>Kai Fan<sup>1</sup>, Jie Qiu<sup>1</sup>, Shuhong Wang<sup>1</sup>, Fang Xu<sup>1</sup>, Weizhi Gong<sup>2</sup>, Zhengjian Cao<sup>2</sup>, Jian Guo Zhu<sup>2</sup>, Youguang Guo<sup>2</sup>, Zhi Wei Lin<sup>2</sup></i> <sup>1</sup> XIAN JIAOTONG UNIVERSITY, P.R. CHINA, <sup>2</sup> INNOPOWER SUPERCONDUCTOR CABLE CO., P.R. CHINA, <sup>3</sup> SYDNEY UNIVERSITY OF TECHNOLOGY, AUSTRALIA	
PF1-13	<b>Analysis of Alternating Magnetic Loss of Divided Nd-Fe-B Sintered Magnets Considering Contact Resistance</b>	501
	<i>Hirofumi Shinagawa<sup>1</sup>, Daisuke Miyagi<sup>1</sup>, Norio Takahashi<sup>1</sup>, Yuhito Doi<sup>2</sup>, Koji Miyata<sup>2</sup></i> <sup>1</sup> OKAYAMA UNIVERSITY, JAPAN, <sup>2</sup> R&D CENTER SHIN-ETSU CHEMICAL CO., JAPAN	

Wednesday, May 14<sup>th</sup>

# A Design for Improving Efficiency through Analyzing Characteristics of Single Phase Line-start Permanent Magnet Motor for Household Appliance

Byeong-Hwa Lee<sup>1</sup>, Fangliang<sup>1</sup>, Jung-Pyo Hong<sup>1</sup>, *Senior Member, IEEE*, Hyuk Nam<sup>2</sup>, and Seung-Hyung Ha<sup>2</sup>

<sup>1</sup> School of Mechanical Engineering, Hanyang University, Seoul 133-791, Korea

<sup>2</sup> LG Electronics, Changwon, Gyeongnam 641-711, Korea

This paper deals with the characteristic analysis and design method of a single-phase line-start permanent magnet (LSPM) motor considering the efficiency and maximum torque with d-and q-axis equivalent circuit and finite element method (FEM). The motor parameters meeting the required efficiency, starting and maximum torque are determined by the characteristic map obtained by the d-q axis equivalent circuit analysis, then the geometric shape design satisfying the motor parameters are performed with FEM. In the end, the improved LSPM motor is fabricated and tested in order to measure the efficiency and maximum torque.

**Index Terms**—Efficiency, equivalent circuit, maximum torque, LSPM motor.

## I. INTRODUCTION

A single-phase induction motor operating with commercial electricity without power electronic switching devices and position sensor is more economical and has higher maintenance than other inverter fed electrical motor [1]. So, it is becoming more generalized as direct operation by supplying the commercial single-phase voltage source of household appliance. However, the motor has problems such as the vibration caused due to unbalanced rotating field of main and subsidiary windings and the difficulty in improving efficiency because of the conductor bar loss [2].

Compared to the single-phase induction motor, a permanent magnet synchronous motor (PMSM) operating at synchronous speed with input frequency has high efficiency and compact size due to PM. However, the PMSM has problems such as high cogging torque and high cost due to PM, switching devices and rotor position sensor. Thus, a single-phase line-start permanent magnet (LSPM) motor complementing the single-phase induction motor and PMSM has been presented. The single-phase LSPM motor is essentially an induction motor added with PM material in rotor part. With the help of PM, efficiency at steady state is increased, but the maximum torque and starting torque, which consists of asynchronous cage torque and magnet braking torque, are decreased [3].

This paper presents a method to improve the efficiency and maximum torque of single-phase LSPM motor through characteristic map obtained by d-and q-axis equivalent circuit analysis. The map indicates the direction of saliency ratio and back-EMF improving the efficiency and maximum torque. And then the prototype LSPM motor is optimized as improved LSPM motor satisfying the given efficiency and maximum torque through design of experiment (DOE) and response surface methodology (RSM). Finally, the characteristic analysis results of improved LSPM motor are compared to those of single-phase induction motor and prototype LSPM motor. Moreover, the improved LSPM motor is fabricated, and the efficiency and maximum torque of the motor are

measured by test.

## II. CHARACTERISTIC ANALYSIS OF SINGLE-PHASE LSPM MOTOR

The configuration and winding connection of a single-phase induction motor and prototype LSPM motor are shown in Fig. 1(a), (b), and (c) respectively. As shown in Fig. 1, both consist of main and subsidiary windings in the stator and conductor bars to produce the starting torque in the rotor. Starting capacitance  $C_s$ , running capacitance  $C_r$ , and positive temperature coefficient (PTC) are connected with the subsidiary windings to increase the starting torque and power factor. Accordingly, it could be considered as a two-phase motor.

### A. Characteristic analysis method of Steady-state

A single-phase induction motor has the unbalanced rotating field due to main and subsidiary windings. The unbalanced field is considered by symmetrical coordinate method. So, the steady state analysis is performed by converting the single-phase LSPM motor into independently two balanced motors [4].

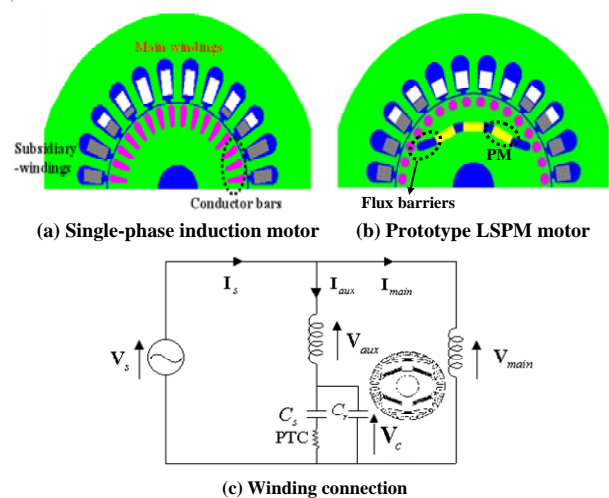


Fig. 1. Single-phase induction motor, prototype LSPM motor and their stator winding connection

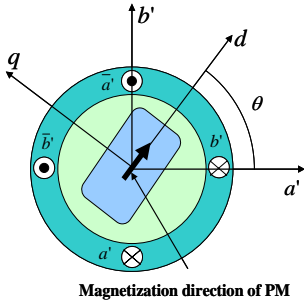


Fig. 2. D- and q-axis relation of stator winding and rotor in two-phase motor

### 1) Voltage equation

In the two-phase motor, d- and q-axis relation between stator winding and rotor is shown in Fig. 2. Form Fig. 2, stator voltage equation is as shown in (1).

$$\begin{bmatrix} v_d \\ v_q \end{bmatrix} = \begin{bmatrix} \cos \theta & \sin \theta \\ -\sin \theta & \cos \theta \end{bmatrix} \begin{bmatrix} v_a' \\ v_b' \end{bmatrix} \quad (1)$$

where  $\theta$  is electrical angle between magnemotive force axis of  $a'$  phase in the stator and d-axis in the rotor.

Also, d- and q-axis voltage equation of two-phase motor expressed as (2).

$$\begin{aligned} v_d &= (R_a' \cos^2 \theta + R_b' \sin^2 \theta) i_d + (-R_a' + R_b') \sin \theta \cos \theta i_q - X_q i_q \\ v_q &= (R_a' \sin^2 \theta + R_b' \cos^2 \theta) i_q + (-R_a' + R_b') \sin \theta \cos \theta i_d + X_d i_d + E \end{aligned} \quad (2)$$

From (2), the current of d- and q-axis is expressed as (3).

$$\begin{aligned} I_d &= \frac{-V_q(R_3 - X_q) + R_2 V_d + E(R_3 - X_q)}{R_1 R_2 - (R_3 + X_d)(R_3 - X_q)} \\ I_q &= \frac{-V_d(R_3 + X_q) + R_2 V_q - E R_1}{R_1 R_2 - (R_3 + X_d)(R_3 - X_q)} \end{aligned} \quad (3)$$

where  $R_1' = R_a' \cos^2 \theta + R_b' \sin^2 \theta$ ,  $R_2' = R_a' \sin^2 \theta + R_b' \cos^2 \theta$ ,  $R_3' = (-R_a' + R_b') \sin \theta \cos \theta$ .

### 2) Calculation of Characteristics

The symmetrical voltage and current components are calculated by the positive and negative impedance [5], and then electrical power and mechanical torque composed of the positive and negative is written as (4).

$$\begin{aligned} P_1 &= (\text{Re}(V_1 I_1^*) - R I_1^2) \longrightarrow T_1 = \frac{P_1}{\omega_s} \\ P_2 &= (\text{Re}(V_2 I_2^*) - R I_2^2) \longrightarrow T_2 = \frac{P_2}{\omega_s} \\ T &= T_1 + T_2 \end{aligned} \quad (4)$$

### 3) Asynchronous characteristic analysis

A single-phase LSPM motor has both induction and synchronous motor characteristics according to the operating condition. The equivalent circuit for single-phase LSPM motor is shown in Fig. 3. Torque under non-synchronous condition is

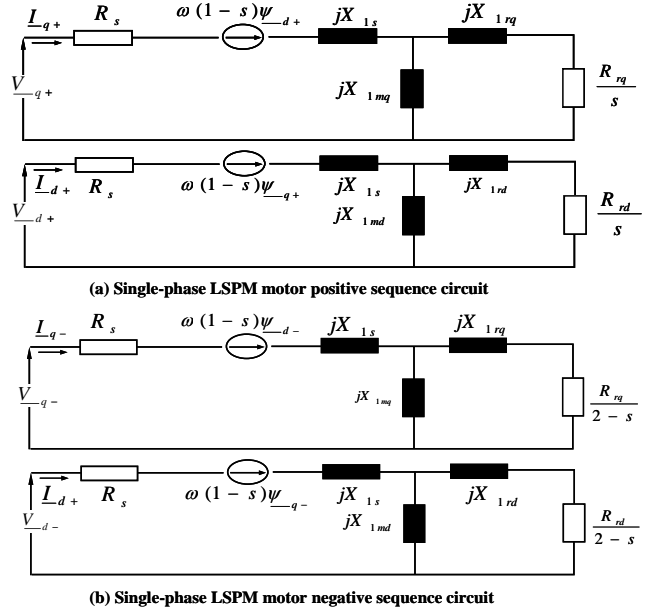


Fig. 3. Single-phase LSPM motor equivalent circuit

divided into cage torque and magnetic torque which are expressed as (5) and (6) respectively.

The starting performances of LSPM motor is dominated by the magnet braking torque and changed according to the section area and shape of conductor bar, usage of PM and the capacity of capacitor.

$$\begin{aligned} T_{(cage)+} &= \frac{P}{2} \cdot \text{Re}[(\underline{\psi}_{-q+})^* \underline{I}_{d+} - (\underline{\psi}_{-d+})^* \underline{I}_{q+}] \\ T_{(cage)-} &= \frac{P}{2} \cdot \text{Re}[(\underline{\psi}_{-q-})^* \underline{I}_{d-} - (\underline{\psi}_{-d-})^* \underline{I}_{q-}] \\ \therefore T_{avg} &= T_{(cage)+} + T_{(cage)-} \end{aligned} \quad (5)$$

$$T_m = \frac{P}{2} \cdot \left[ \frac{1}{\beta} \cdot \psi_{dm} I_{qm} - \beta \cdot \psi_{qm} I_{dm} \right] \quad (6)$$

The average air-gap resultant electromagnetic torque is given by (7), and Fig. 4 shows each torque and starting capacitor is off when the slip is 0.2

$$T_e = T_{avg} + T_m \quad (7)$$

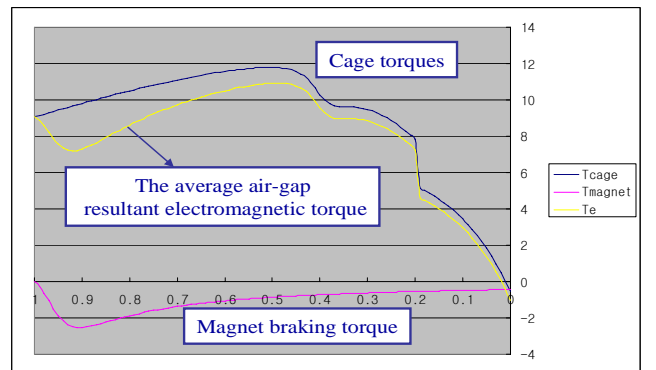


Fig. 4. The average air-gap resultant electromagnetic torque

### III. DESIGN AND ANALYSIS RESULT

Except for the shape of the conductor bars and the usage of PM, the stator and rotor shape of prototype LSPM motor are the same compared with the single-phase induction motor. Compared to the induction motor, the efficiency of prototype LSPM motor is increased about 5% due to the loss reduction at the conductor bars, but the maximum torque is decreased about 12%. Therefore, this paper designs the LSPM motor improving the efficiency and maximum torque as compared with the induction motor.

The characteristic map obtained by the equivalent circuit shows the response of the efficiency and maximum torque according to the change of saliency ratio, back-EMF and d- and q-axis inductance and is given in Fig. 6. The d- and q-axis inductance are calculated under the constant current angle, and the maximum torque is estimated as follows:

$$\begin{aligned} T &= P_n \left[ \psi_a i_q + (L_d - L_q) i_d i_q \right] \\ &= T_m + T_r \end{aligned} \quad (8)$$

The maximum torque is increased as back-EMF is great, and d-axis is decreased when the saliency ratio is constant. Therefore, the increase direction of the maximum torque is shown in Fig. 6(a), (c) and (e).

The calculation of the efficiency is expressed as (9) and the core and mechanical loss are ignored.

$$Eff. = \frac{P_{out}}{P_{out} + P_{loss}} \times 100 [\%] \quad (9)$$

where,  $P_{out}$  is mechanical output and  $P_{loss}$  is the copper loss.

The efficiency is increased as back-EMF or d-axis inductance is great when the saliency ratio is constant. Thus, the increase direction of efficiency is shown in Fig. 6(b), (c) and (f).

The region satisfying the efficiency and maximum torque as the saliency ratio is increased is expanded. As the saliency ratio grows, the maximum torque is increased, because the effect by the difference of d- and q-axis inductance is bigger than the effect by the decrease of  $i_q$ . The region to satisfy the efficiency is expanded, because the copper loss is decreased by the reduction of  $i_q$ . The design to satisfy both the efficiency and the maximum torque is difficult, because the increase direction of the efficiency and maximum torque is opposite. Therefore, in the initial design stage, the characteristic map is very important in order to determine the design direction. From the result of characteristic map, the efficiency of prototype LSPM motor satisfies the required efficiency, but the maximum torque is not. Therefore, back EMF and salient ratio to satisfy the characteristics of prototype LSPM motor should be enhanced.

The optimal design as regards the double-layer shape based on prototype LSPM motor is performed, because the region satisfying the characteristics due to the increase of saliency ratio is expanded, and design parameters are shown in Fig. 7.

The effects of design factors concerning back-EMF and saliency ratio obtained by DOE are shown in Fig. 8.  $L_{pm1}$  and  $G_{pm}$  mainly affect the back-EMF and the saliency ratio, So RSM is firstly performed by the two design factors and the

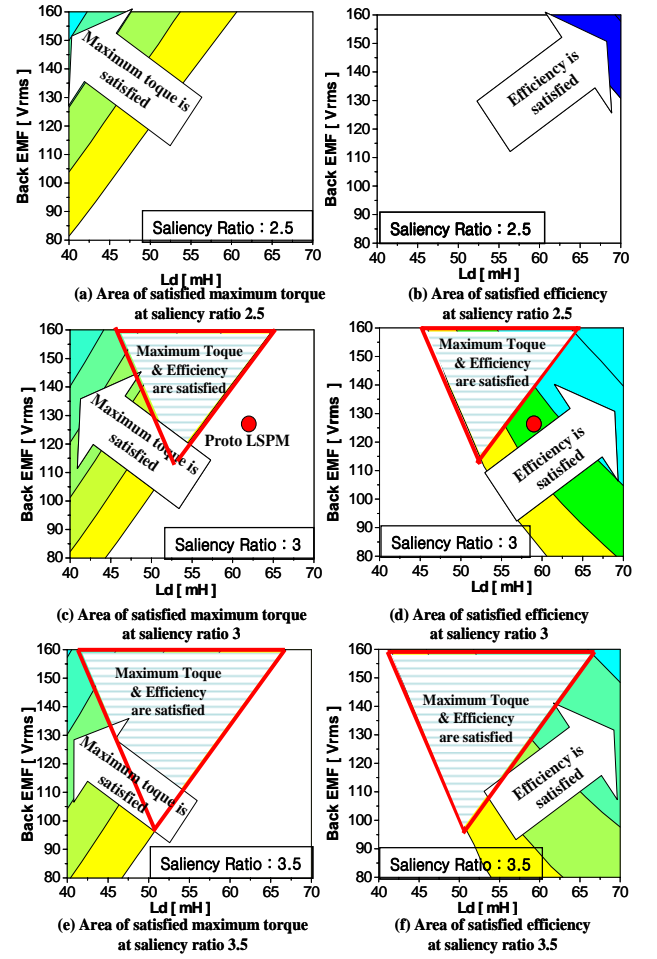


Fig. 6 Characteristic map

objective function and constraint condition are defined as follows:

- Objective function:

$$\text{Efficiency} > 90 [\%], \text{Maximum torque} > 130 [\text{kgfcm}]$$

- Subject to:

$$\text{Output} > 2 [\text{kW}], \text{starting torque} > 26 [\text{kgfcm}]$$

RSM is secondly performed by  $P_{spm}$ , PM position in the layer 1 and layer 2, and  $A_{fb2}$ , the angle of flux-barrier in layer 2.

Both the back-EMF and the salient ratio as shown in Fig. 9 are satisfied with the efficiency and maximum torque when  $L_{pm1}$  and  $G_{pm}$  are 7.0 mm and 2.6 mm, and  $P_{spm}$  and  $A_{fb2}$  are 0 mm and  $22.06^\circ$ , respectively. The motor parameters of improved LSPM motor estimated by FEM are shown in table I and they are in the region of characteristic map satisfying the efficiency and the maximum torque.

The steady state characteristics are analyzed by FEM, and the relative comparisons between single phase induction motor and improved LSPM motor are shown in Fig. 10(a). In comparison with the induction motor, the efficiency of improved LSPM motor is increased about 5% due to the reduction of conductor bar loss, and the synchronous speed is extended from 2867rpm to 3000rpm. The experimental results

of single-phase induction motor and improved LSPM motor are shown in Fig. 10(b). From the comparison, the improved LSPM motor satisfies maximum torque and synchronous speed, and the efficiency is increased about 4.3% than the single-phase induction motor. The starting performance of improved LSPM motor is shown in Fig. 11.

IV. CONCLUSIONS

In this paper, the design method to improve the characteristics of prototype LSPM motor is presented. The characteristics are investigated with the equivalent circuit according to the change of motor parameters. Moreover, the main design factors related to the characteristics are selected by DOE, and the optimal design is performed with them. In the end, the validity of the method is verified by test.

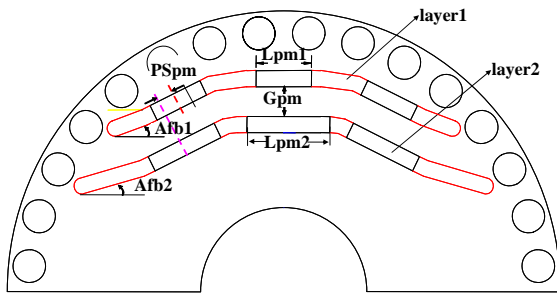


Fig. 7. Design parameter

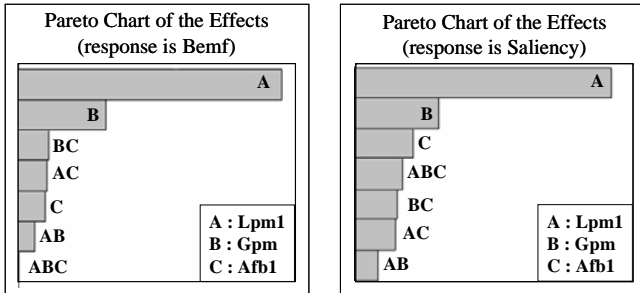


Fig. 8. Effect of design factor of back-EMF and saliency ratio

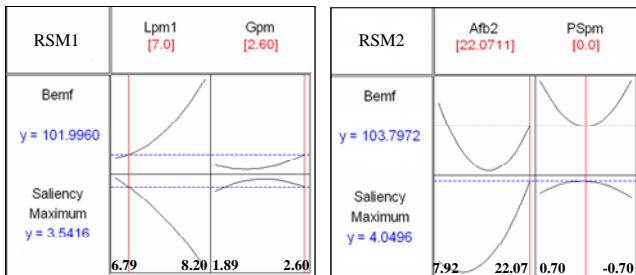
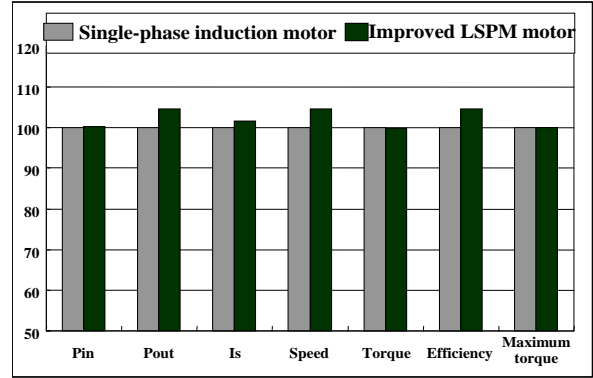


Fig. 9. Response surface of back-EMF and saliency ratio

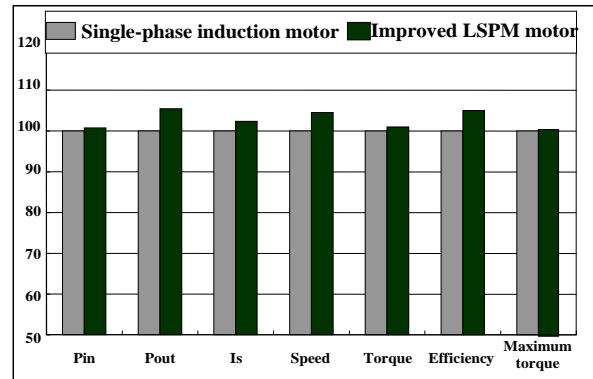
TABLE I

COMPARISON OF MOTOR PARAMETERS

	Back EMF[Vrms]	Ld [mH]	Lq [mH]	Saliency ratio
Proto LSPM	125	63	186.48	2.96
Improved LSPM	103	53	187.62	3.54



(a) Result of FEA



(b) Result of Experiment

Fig. 10 Comparison of result

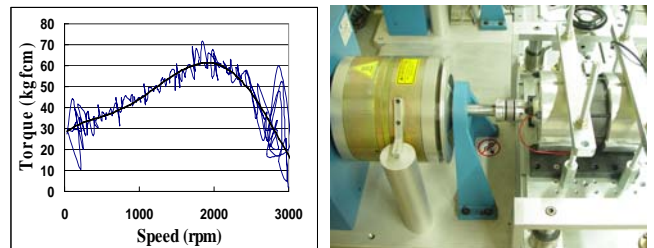


Fig. 11. Experimental result of LSPRM motor and test set

REFERENCES

- [1] T. J. E. Miller, "Single-phase permanent magnet motor analysis," *IEEE Trans. Ind. Applicat.*, no. 4, pp. 651-658, 1985
- [2] H. Nam, K. H. Ha, J. J. Lee, J. P. Hong, and G. H. Kang, "A study on iron loss analysis method considering the harmonics of the flux density waveform using iron loss curves tested on Epstein samples," *IEEE Trans. Magn.*, vol. 39, pp. 1472-1475, May 2003.
- [3] Mircea Popescu, *Senior Member, IEEE*, T. J. E. Miller, *Fellow, IEEE*, "Asynchronous Performance Analysis of a Single-Phase Capacitor-Start, Capacitor-Run Permanent Magnet Motor", *IEEE Trans. On Energy covers.* vol. 20, NO. 1, March 2005.
- [4] G. H. Kang, J. Hur, H. Nam, J. P. Hong, and G. T. Kim, "Analysis of irreversible magnet demagnetization in line-start motors based on the finite-element method," *IEEE Trans.* vol. 39, NO. 3, pp. 1488-1491, May 2003.
- [5] G. H. Kang, J. Hur, H. Nam, J. P. Hong, and J. Hur, "Analysis and Design Methodology for Single-Phase Line-start Permanent Magnet Motor Considering Parameters Variation on d-q Axis Vector Diagram," *Industry Applications Conference*, 2003. 38th IAS Annual Meeting. Conference Record of the Vol. 3, pp. 1946 - 1953, Oct. 2003.